PHYSICAL REVIEW B VOLUME 24, NUMBER 2 15 JULY 1981

Calculation of optical spectra of aluminum

Frank Szmulowicz* and Benjamin Segall†
Case Western Reserve University, Cleveland, Ohio 44106
(Received 2 September 1980)

The electronic structure and optical properties of aluminum were studied using the augmented-plane-wave (APW) method. To improve the agreement between the calculated electronic structure and experiment a semiempirical scheme of Chen and Segall was used to adjust the band structure. This parametrization was implemented by employing a few pieces of experimental data on de Haas–van Alphen cross sections, the position of a major optical peak and the bandwidth of Al. The parametrized bands and wave functions were used in a calculation of the dielectric constant of Al in which the dipole matrix elements were included. The spectrum was analyzed with regard to the origin of structure in $\vec{k}$ space, with major structures treated analytically using the pseudopotential model. A novel aspect of this work is the elucidation of small-frequency behavior of the imaginary part of the dielectric constant which was shown to be nonzero at low frequencies due to an accidental degeneracy (in the absence of spin-orbit splitting) of the bands on the ΓKWX plane. The calculated spectrum is in very good agreement with optical data with respect to the location, strength, and width of major structures. A comparison between momentum matrix elements calculated by the pseudopotential and APW method is presented.

I. INTRODUCTION

In this work we study the electronic structure and the associated optical properties of Al by the augmented-plane-wave (APW) method. It has been frequently found that the one-electron excitation spectra calculated using conventional potentials, e.g., the so-called $X\alpha$ potentials, are not too accurate; indeed, we will find that to be the case here. Because of this we resort to a semiempirical approach. The approach used, a variant of the one introduced by Chen and Segall (CS)[1] in a study of Cu and Ag, involves a convenient adjustment of the logarithmic derivatives obtained in a previous *a priori* calculation. The adjustments are made to fit a small number of empirical data. Since the relevant data for Al, and other polyvalent metals with nearly-free electronlike bands, are different from those involved in the noble metals, this work can in part be considered a test of the feasibility of applying the parametrization scheme to this other class of band structures.

There have been an appreciable number of band calculations of Al [Refs. 2–6(b)], the results of which differ only by relatively small amounts for the occupied and low-lying excited states and which lead to Fermi surfaces in reasonably good accord with experiments.[6(a),7] It is thus clear that the band structure of Al is generally well known. The optical response of this metal has also been studied a few times.[8–12] The first study, which was by Ehrenreich *et al.*[9] in 1963 was, in fact, one of the first detailed investigations of the optical properties of a metal. There the 1.6-eV peak of $\epsilon_2(\omega)$ was shown to arise from the large region of $\vec{k}$ space associated with the approximately parallel bands in the neighborhood of the Σ axis—the first example of what was later termed the "parallel" band effect. A full calculation of the interband contribution to ϵ_2 was not undertaken; only a rough estimate of the contributions in the region of the peak was made.[10] Subsequently Dresselhaus *et al.*[11] and Brust[8] made complete computations of $\epsilon_2^b(\omega)$ [i.e., involving sums over the complete Brillouin zone (BZ)] using the pseudopotential method with potential coefficients $V(1,1,1)$ and $V(2,0,0)$ found by Ashcroft[6(a)] to produce a Fermi surface in close agreement with that deduced from de Haas–van Alphen measurements. These calculations were successful in producing another strong peak in the interband part of $\epsilon_2(\omega)$ [$\epsilon_2^b(\omega)$] at 0.5 eV which had been found in the measured spectrum and which was attributed to another pair of parallel bands. The ϵ_2^b obtained in these works were in general agreement with the measured spectrum. Ashcroft and Sturm,[12] in a study of the parallel-band effect, obtained analytic expressions for $\sigma_1^b(\omega)$ using a two-plane-wave model which included momentum matrix elements and a relaxation time and showed that the appropriately weighted sum of such terms for the $V(1,1,1)$ and $V(2,0,0)$ interactions reproduce the principal features in the spectrum of Al.

One of the principal motivations for this work is to provide the first complete and systematic calculation of the optical properties of Al with a method which employs the full potential (in contrast to a pseudopotential). In addition to its value *per se*, this work could provide a useful comparison with the pseudopotential results[8,11,12]

 © 1981 The American Physical Society

on this important material which is a prototype of the polyvalent nearly-free-electron metals. For while the pseudopotential was chosen to accurately fit the $E_n(\vec{k})$ at the Fermi energy (E_F), there is less certainty about the accuracy of states with energies reasonably far from E_F, and also there is some uncertainty about the accuracy of the momentum matrix elements computed by the simple scheme. Finally, subsequent to those calculations, new experimental data have appeared on the optical properties[13-15] and the Fermi surface.[7]

The paper is organized as follows. The computation procedures and their tests are presented in Sec. II. Section III contains a description of the parametrization of Al's bands and a presentation of the resulting band structure. Section IV deals with the calculated optical response functions, its comparison with measurements, and the analytical treatment of the low-frequency behavior of $\epsilon_2^b(\omega)$. Conclusions are presented in Sec. V.

II. COMPUTATIONAL PROCEDURES

The augmented-plane-wave (APW) method, introduced by Slater,[16] was employed to obtain the energy eigenvalues and wave functions. In the conventional application of the APW method, the potential is taken to have the muffin-tin form. This form provides a good approximation for the potential for a cubic-close-packed structure. The muffin-tin potential was obtained by suitable averaging of the potential given by the Mattheiss prescription,[17,18] that is, by the sum of spherically symmetric atomic potentials centered at the lattice sites and a local density exchange-correlation contribution (i.e., the so-called $X\alpha$ contribution) with $\alpha = 1$.

The wave-function expansion in plane waves in the region $r > r_M$ (the muffin-tin radius) was carried out using reciprocal-lattice vectors $\vec{K}_i$ satisfying

$$|\vec{k}_i|^2 = |\vec{k} + \vec{K}_i|^2 \leq 11.0(2\pi/a)^2 , \tag{1}$$

where a is the lattice constant, while the expansion in harmonics, for $r < r_M$, included terms up to $l = 10$. According to Switendick's empirical rules[19] this should produce bands converged to within 10^{-3} Ry. The eigenvalue problem was carried out at 89 $\vec{k}$ points in the irreducible wedge of the fcc BZ. Gaussian elimination with pivoting was used to solve the secular equation, and the coefficients of the wave function were obtained by back substitution. Group-theoretical techniques were employed to reduce the size of the secular equation and to improve the accuracy for all $\vec{k}$ having symmetry. The results of our APW program were checked against the calculations of Cu by Segall[20] and Burdick[21] and against the calculation of Al by Segall.[4] These comparisons indicated that the present results are accurate to within 0.001 Ry.

A complete calculation of the optical spectrum [e.g., $\epsilon_2(\omega)$ and $\epsilon_1(\omega)$] requires the computation of matrix elements of the momentum operator (MEM). Probably the simplest way to obtain the APW MEM is in terms of the matrix elements of $\vec{\nabla} V$ (which follows from $-i\hbar\vec{P}_{fi} = \langle f | [H, \vec{P}] | i \rangle$), for then the contribution from $r > r_M$ vanishes. However, we decided against its use for several reasons. First, the values become relatively inaccurate for close-lying states because of the occurrence of the energy difference in the denominator. More important is the fact that we ultimately employ a nonlocal l-dependent potential (associated with a parametrization) and this leads to a commutator which is too cumbersome. Instead we evaluated the MEM directly in terms of the APW wave functions throughout the cell. This approach also permits us to evaluate diagonal MEM which we need for the interpolation scheme to be discussed below and which cannot be obtained from the $\vec{\nabla} V$ approach. Our MEM computations were checked against the MEM for Cu obtained by Janak *et al.*[22] and Chen[23] and were found to be in very close agreement. The $(\text{MEM})^2$ were found to be converged to within 0.001 Ry using at most $l = 5$ components.

Since we were able to compute the APW MEM quite accurately and since there have appeared widely conflicting reports about the accuracy of MEM computed with pseudopotential wave functions,[24-27] we decided to investigate this question for the low-lying bands in Al. In brief, we found that for the larger matrix elements the pseudopotential values were typically in error only by about 5%, although a few errors as large as 20% were also found. That these MEM's are relatively satisfactory is probably connected with the fact that the core is rather small in Al. It seems probable that the results would be less satisfactory in materials with larger cores (e.g., Zn). For the smaller MEM larger relative errors appeared. Details of how these computations were carried out and specific results appear in Appendix A.

The Gilat-Raubenheimer (GR) method was used to carry out the $\vec{k}$-space sums which occur in the evaluation of the density of states, the imaginary part of the dielectric constant, $\epsilon_2(\omega)$, and the volume integral used to determine the Fermi energy.[28] The irreducible wedge in the BZ was subdivided into 10100 small cubes. The energies

and energy gradients at the center of these cubes were obtained by a $\vec{k}\cdot\vec{p}$ interpolation from the mesh of 89 $\vec{k}$ points in the wedge on which *ab initio* energies and MEM were calculated. To ensure that accurate values were obtained for these quantities for the first four bands on the finer mesh, the *ab initio* values on the first six bands were used. The density-of-states program was checked against known analytic results for the density of states of the fcc tight-binding s band.[29] Excellent agreement was found. Even the strong singularities in the exact result, which were not encountered in realistic cases, were very satisfactorily reproduced.

The calculation of $\epsilon_2(\omega)$ entails the same type of surface integral encountered in the density of states and, of course, includes a transition probability factor. Appropriate analytic expressions were included to take account of the corrections required when one or both bands involved in the transition is cut by the Fermi surface in a cube. The $\epsilon_2(\omega)$ program was checked against an analytic result having a cusp structure for a two-band model appropriate to the interconduction transitions at L.[30] With a 5950-cube subdivision of the wedge, a graph of the numerically computed result could not be distinguished from that of the analytic result. In addition, the Fermi energy was determined by a variant of the GR scheme which uses analytic expressions for the volume rather than the surface areas.

With the $\vec{k}\cdot\vec{p}$ interpolation scheme energies on the fine mesh could be obtained with an accuracy of a few mRy. More importantly, this determinantal scheme is capable of accurately reproducing the bands around crossings and degeneracies.

III. PARAMETRIZATION AND BAND-STRUCTURE RESULTS

The energy bands along symmetry directions obtained with the potential discussed above are shown as the dashed curves in Fig. 1. It can be seen immediately from the fact that the $\Sigma_1-\Sigma_3$ gap around E_F is only about 0.8 eV that these $E_n(\vec{k})$ are not as accurate as desired. This gap which is known to be the energy of the principal peak in $\epsilon_2(\omega)$ should be 1.6 eV (see below). Such discrepancies which are found frequently in the excitation spectra of solids are associated with uncertainties in the effective potential, in particular, with the exchange and correlation contributions (in general, a nonlocal energy-dependent self-energy). On the other hand, it is known that ground-state properties are satisfactorily reproduced by self-consistent calculations in the

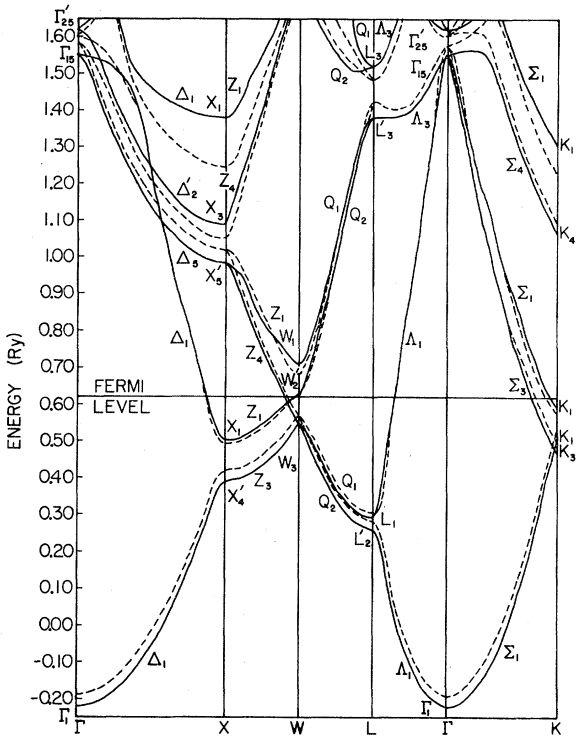

FIG. 1. Al band structure along important symmetry directions (parametrized bands—solid lines, unparametrized bands—dashed lines).

local-density-functional (LDF) theory with suitable exchange and correlation terms [e.g., those of von Barth and Hedin[31(a)]]. But there is considerable evidence that this theory, which is designed for the ground state, does not yield accurate excited states.[31(b)] It is well known, for example, that such calculations are considerably less successful in determining the forbidden band gaps of semiconductors and insulators.[31(c)] Two options were open to us. We could have done a self-consistent local density calculation with little assurance that the excitation spectra would be given correctly or we could utilize a parametrization approach. We chose the latter alternative.

The approach we employed was a variant of the one used by Chen and Segall[1] (CS) for the noble metals. They found it convenient to work with the logarithmic derivatives $L_l(E)=R_l'(r_M,E)/R_l(r_M,E)$ as the relevant potential quantities. Also, they noted that though the $L_l(E)$ obtained in a reasonable *ab initio* calculation, henceforth denoted $L_l^{(0)}(E)$, were not quantitatively as accurate as desired, they always have the correct general energy dependence. Thus only a small rigid shift relative to the E axis plus a weak distortion for each l are needed to reproduce a set

of $L_l(E)$ which would yield correct energies. These operations could be affected simply by introducing $v_l(E)$ such that

$$L_l(E) = L_l^{(0)}(E + v_l(E)). \tag{2}$$

It was also shown that starting with any reasonable potential $V^{(0)}(r)$ the required $v_l(E)$ would be weakly dependent on E over a large range and thus be readily parametrized, e.g., by low-order polynomials. Thus by adjusting the parameters in the $v_l(E)$, and hence the $L_l(E)$, to yield agreement with only a few pieces of empirical data one obtains the correct $L_l(E)$ over a relatively large energy range. We note that only the L_l for $l = 0$, 1, and 2 are to be altered in this work.

It is clear that there is not a unique effective potential $\tilde{V}_l(r, E) = V^{(0)}(r) + \Delta V_l(r, E)$ (or correction ΔV_l) corresponding to a $L_l(E)$ specified over a finite range of E. Thus, it appears that in principle one cannot obtain radial functions corresponding to the empirically corrected $L_l(E)$. We should note, however, that among the infinite number of possible $\Delta V_l(r, E)$ there is a particularly simple one, namely, the square-well potential of depth $v_l(E)$. The corresponding radial function is just $R_l^{(0)}(r, E + v_l(E))$, where $R_l^{(0)}(r, E)$ is the radial solution for $V^{(0)}(r)$ at energy E. CS argued that for the weak and smooth $v_l(E)$ involved, these functions must be reasonably good approximations to the correct functions and demonstrated the point with a number of examples including the computation of MEM.[32] In this work we require wave functions to evaluate the MEM and thus use these solutions.

In the parametrization for a metal it is clearly advantageous to utilize the Fermi-surface data to accurately correct the L_l at E_F which is essentially the middle of the energy range of interest. For this purpose we use calipers of the second- and third-zone surfaces taken from the Anderson and Lane four-OPW (orthogonalized-plane-wave) fit of their high-frequency[7] and the Larson and Gordon low-frequency[33] dHvA measurements. Details of how this was carried out are given in Appendix B. We only note here that six separate calipers were accurately fitted in the determination of the three $v_l(E_F)$ which have an estimated uncertainty of about 1 mRy.

Two other inputs were made. The first was the occupied band width which relates to v_0 since the bottom of the band is an s state (Γ_1). For the experimental value we used the 11.5 eV obtained by Neddermeyer and Wiech from their L_{23} emission spectrum,[34] which, of course, is sensitive to the s component. The v_0 is adjusted to locate the Γ_1 level at $E_F - 11.5$ eV. The last input, which is very important to this work, is the 1.60-eV position of the ϵ_2 peak determined by the Bos and Lynch[13] 4.3-K absorption measurements. As already noted, it was found in the early work[9] that this peak arose from regions in $\vec{k}$ space in the ΓKWX plane around the Σ axis where the two bands are quite parallel. The 1.60 eV then is equal to the $\Sigma_1 - \Sigma_3$ gap for $\vec{k}$ such that $E(\Sigma_3) = E_F$. Now, the question is which of the three v_l should be adjusted (Σ_1 contains all l). It

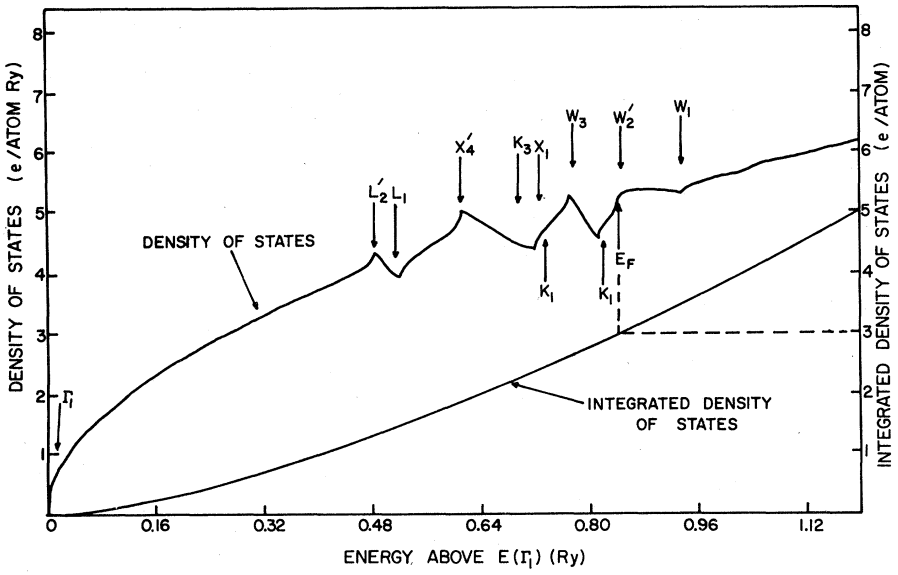

FIG. 2. Density of states and integrated density of states for Al. The symbols indicate the symmetry states giving rise to the critical points in the density of states.

TABLE I. Energies (in Ry) at selected high-symmetry points in the Brillouin zone for the parametrized bands of Al.

Γ	Energy	X	Energy	W	Energy	K	Energy	L	
Γ_1	−0.222	X_4'	0.390	W_3	0.554	K_3	0.473	L_2'	0.260
Γ_{15}	1.555	X_1	0.505	W_2'	0.626	K_1	0.513	L_1	0.294
Γ_{25}'	1.620	X_5'	0.987	W_1	0.713	K_1	0.598	L_3'	1.382
Γ_2'	1.879	X_3	1.089	W_2'	1.749	K_4	1.064	L_3	1.521
		X_1	1.382	W_3	1.810	K_1	1.301	L_2'	1.729
						K_1	1.777		

seemed most reasonable to adjust the v_0 [so that $E(\Sigma_1)=E_F+1.60$ eV] as we then could fit the $v_0(E)$ by a quadratic function over the relatively large range of 15 eV or so. The $v_l(E)$ for $l=1$ and 2 are given by constants.

The bands obtained from the parametrization are displayed in Fig. 1 as the solid curves. Values of the energies of symmetry states up to about 1.9 Ry are given in Table I. In Fig. 2 we show the density of states $D(E)$ and the integrated density of states. Each structure appearing in $D(E)$ is labeled with the state producing it. We find that $D(E_F)=5.300$ (atom Ry)$^{-1}$. When combined with the experimentally determined linear coefficient of the specific heat,[35] $\gamma=1.35+0.01$ mJ/mole K^2, this yields a mass enhancement factor of 1.47. This value is comparable to (but slightly smaller than) the enhancements of the cyclotron masses[7] and to the calculated enhancements due to the electron-phonon interaction.[36]

As checks on the parametrization we calculated the areas for the $\psi_1(1,1,0)$ and $\xi(1,0,0)$ orbits (notation[7] of Anderson and Lane) and obtained, respectively, 1.707 and 0.351 in units of $(2\pi/a)^2$. The corresponding experimental areas are 1.709 and 0.347. The agreement is very good considering the sensitivity of the $\xi(100)$, which is on the UWX face, to small changes in the potential which can alter the connectivity of the third zone around W. We also recalculated the E_F, finding a new value of 0.6226 Ry which is only slightly below the unparametrized value of 0.6234 Ry. The degree to which other aspects of the calculated optical properties agree with experiment will provide additional checks on the parametrization. These will be considered below.

IV. RESULTS

The response of an electronic system to an electromagnetic wave of frequency ω can be described by complex dielectric constant $\epsilon(\vec{q},\omega)$ with $q\simeq 0$ in the "optical" range. It is useful to divide ϵ into contributions from the intraband (f) and interband (b) transitions[37]

$$\epsilon(\omega)=\epsilon^f(\omega)+\epsilon^b(\omega)=\epsilon^f(\omega)+\epsilon_1^b(\omega)+i\epsilon_2^b(\omega). \tag{3}$$

The former is usually given in terms of the expression for the Drude model

$$\epsilon^f(\omega)=1-\frac{\omega_{pa}^2}{\omega(\omega+i/\tau)}, \tag{4}$$

where $\omega_{pa}^2=4\pi n_c e^2/m_a$, n_c is the conduction-electron density, m_a the so-called optical mass, and τ the relaxation time.

In the limit of vanishing linewidth, ϵ_2^b is given by

$$\epsilon_2^b(\omega)=\frac{4\pi^2e^2}{3}(m^2\omega^2)^{-1}\times\sum_{l,n}\int_{\mathrm{BZ}}\frac{2}{(2\pi)^3}d^3k\,|\vec{P}_{ln}|^2\delta(E_l(\vec{k})-E_n(\vec{k})-\hbar\omega), \tag{5}$$

where the sum and integral are restricted so that the state $\vec{k}$ in band n (l) is unoccupied (occupied).[37] As is well known, $\epsilon_1(\omega)$, which can also be ex-

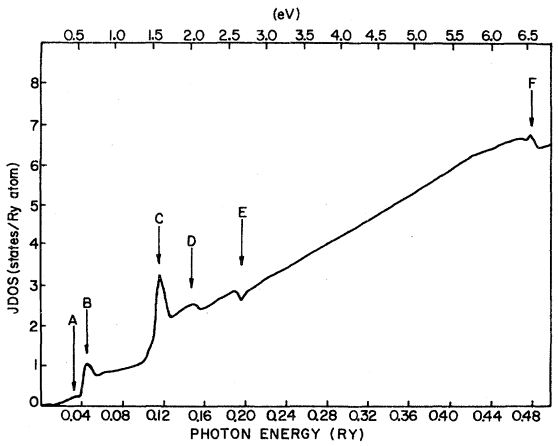

FIG. 3. JDOS for Al. The arrows point to the locations of structure in the curve.

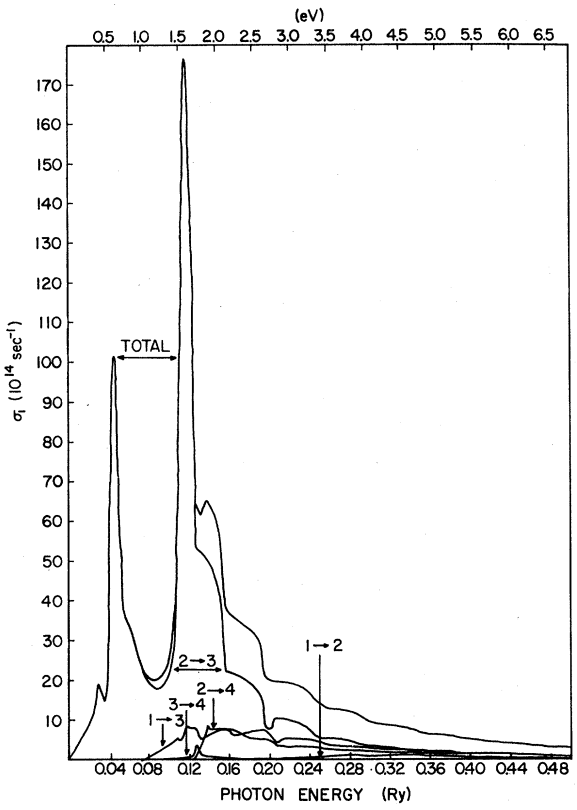

FIG. 4. Real part of the interband conductivity for Al and its decomposition by contributions from various interband transitions.

pressed in terms of a BZ integral and sum over bands of "oscillator"-like terms, can be obtained from $\epsilon_2(\omega)$ by a Kramers-Kronig relation. When the MEM in Eq. (5) is taken to be constant the resulting quantity is proportional to the unbroadened joint density of states [JDOS, $\mathcal{J}(\omega)$]. This function for Al is displayed in Fig. 3 while the real part of interband conductivity, $\sigma_1^b(\omega)$ $[=\omega\epsilon_2^b(\omega)/4\pi]$ along with its decomposition into

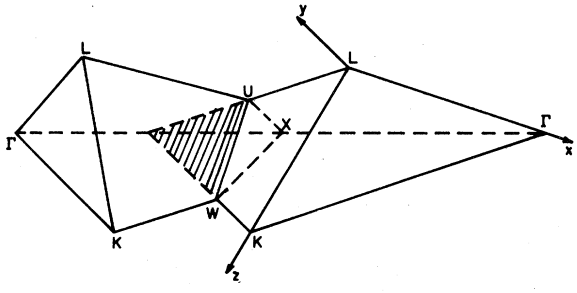

FIG. 5. Plot of two adjoining irreducible wedges, with the extension of the (1,1,1) face of one wedge into the other marked by the stripes. The x, y, and z axes are used as the coordinate system for the analysis of the 0.5-eV peak in $\epsilon_2^b(\omega)$ of Al.

the various interband $(i \to j)$ contributions is shown in Fig. 4.

We have studied the origins of the structures labeled A, B, C, D, E, and F. It is seen that A and B arise from $2 \to 3$ transitions and, further, it is found that they come from the same region of the BZ. A results from the Fermi-energy cutoff which produces the decrease in $\mathcal{J}(\omega)$. The origin of the peak B at 0.5 eV can be understood in terms of a simple two-plane-wave model. It is first noted that the two free-electron states $\exp[i(\vec{k}+\vec{K}_n)\cdot\vec{r}]$ with reciprocal-lattice vectors $(2\pi/a)(\bar{1},\bar{1},\bar{1})$ and $(2\pi/a)(0,0,\bar{2})$ are degenerate over the plane given by

$$k_z - k_x - k_y = \pi/a\,, \tag{6}$$

which is shown as the shaded region in Fig. 5. The degeneracy is lifted by the potential and it is easily shown that the interband separation for any point on the plane is $\omega(\vec{k}) = 2V(1,1,1) \simeq 0.05$ Ry where $V(\vec{K}_n)$ is the Fourier component of the pseudopotential. In the realistic band structure the two bands are not exactly parallel. Also, the interband surface must bend around in order to contact the symmetry planes UWX, ΓKWX, and ΓLUX at right angles, and the point of contact of the second and third bands is moved from W to a point on the Z axis (see Figs. 1 and 6).

A similar analysis can be carried out for the structure C at 1.6 eV. The plane waves with $(a/2\pi)\vec{K}_n = (\bar{1},\bar{1},\bar{1})$ and $(1,\bar{1},\bar{1})$ are degenerate over the whole ΓKWX plane. The potential splits the degeneracy by $2V(200) \cong 1.6$ eV with the resulting bands giving rise to small gradients in the interband energy and a singularity in the JDOS. The Fermi condition is satisfied only in the vicinity of the Σ axis. As noted in Sec. I, it was in the consideration of the contribution from these transitions that the so-called parallel-band effect

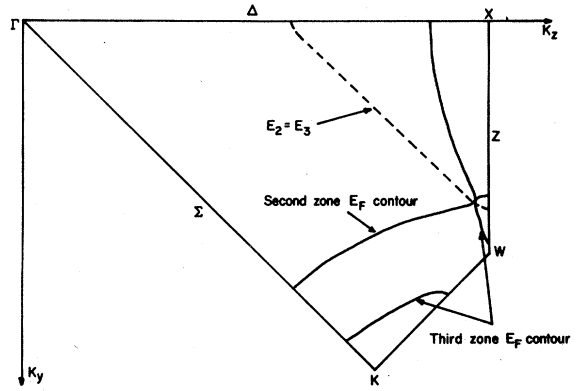

FIG. 6. Fermi-surface contours for the second and third zones, and the line of degeneracy of the second and third bands, on the ΓKWX plane.

was in fact first noted.[9] We will return to the contributions of B and C to $\mathcal{J}(\omega)$ after discussing the structures D, E, and F.

Structure D, which was also identified by Ehrenreich *et al.*,[9] is due to the onset of transitions from band 2 to 4 in the vicinity of point W(i.e., $W_3 \rightarrow W_1$). The next structure, E, arises from the cutoff by Fermi factors of band 2 to 4 transitions involving general points in the vicinity of the UWX plane. Finally, F results from band 2 to 4 transitions at X ($X_1 \rightarrow X_5'$). Since this occurs at high ω, the structure in ϵ_2^b will be very weak because $\epsilon_2 \alpha \mathcal{J}(\omega)/\omega^{-2}$ and also because the broadening increases with ω.

The contribution to JDOS from the approximate "parallel" band structures associated with B and C considered above are easily evaluated. We take the y and z components of $\vec{k}$ to lie in the plane and the x component normal to it as is indicated in Fig. 5 for B. For C we take the z axis along Σ, the y axis normal to it in the ΓKWX plane through the point X (which is thus the origin) on the extension of Σ in the next zone, and again the x axis perpendicular to the plane. For small x (which is measured from the plane in both cases) the bands are given by

$$E_{+(-)} = \alpha_{\parallel}(y^2 + z^2) \pm [V(K) + \alpha_{\perp}^{+(-)} x^2] \tag{7a}$$

and $\omega(\vec{k}) = E_+ - E_- = 2V + (\alpha_{\perp}^{(+)} + \alpha_{\perp}^{(-)})x^2$. The quadratic forms in Eq. (7a) results from fcc symmetry and the symmetry of the simple two-band model. Using cylindrical coordinates with $\rho^2 = y^2 + z^2$ the JDOS takes the form

$$\mathcal{J}(\omega) \int dx \int_{\rho_1}^{\rho_2} 2\pi\rho \, d\rho \, \delta(\omega - [2V + (\alpha_{\perp}^{+} + \alpha_{\perp}^{-})x^2]) \tag{7b}$$

with

$$\alpha_{\parallel} \rho_{1(2)}^2 = E_F - (+)(V + \alpha^{+(-)} x^2) ,$$

where the limits represent the Fermi cutoff condition. The integral is easily carried out to show that for ω not too far from the edge (the range to which the above approximation is limited)

$$\mathcal{J}(\omega) \propto \omega(\omega - 2V)^{-1/2} \tag{8}$$

and, of course, vanishes for $\omega < 2V$. The singular structure, which results from the relatively large part of the zone involved, is moderated in the real band structure by the fact that the bands are not exactly parallel. Harrison[38] was the first to obtain Eq. (8). A much more complete analytic description of the optical response around the peak in the single-plane approximation was carried out by Ashcroft and Sturm[12] (AS). They included matrix elements (in the pseudopotential approximation) and a phenomenological relaxation time, and their expressions are valid over a larger energy range than is Eq. (8). In the $\tau \rightarrow \infty$ limit their result exhibits the same singularity as given above.

A. Comparison with experiment

The comparison between the calculated and experimentally obtained σ_1^b is presented in Fig. 7. The theoretical curve was obtained by broadening the result shown in Fig. 4 by a Lorentzian having a full width at half maximum $\Gamma(\omega) = (a + b\omega)^{1/2}$ with $a = 1.852 \times 10^{-6}$ Ry^2 and $b = 2.314 \times 10^{-4}$ Ry chosen so as to yield the magnitudes of the experimental peaks. The form of Γ was chosen, admittedly somewhat arbitrarily, as it increases slowly with ω. The $\sigma_1^b(\omega)$ up to 3 eV was obtained by Benbow and Lynch[14] (BL) from their 4.2-K absorptance measurements by Kramers-Kronig analysis and subtraction of the intraband (Drude) component.[39] The higher ω values are from Hagemann *et al.*[40] The difference between the two empirical curves in their region of overlap could, in part, be due to the fact that the low-energy measurements were made at 4.2 K while the other was at room temperature.

It can be seen that the agreement with the empirical result is generally good both in magnitude and shape. We start the more detailed comparison with the more featureless part of the spectrum, the part above the second peak. Above 3.0 eV the agreement is very good, but below that the data do not exhibit the undulations in the calculated σ_1^b, which are the vestiges of the D and E structures. This suggests that our $\Gamma(\omega)$ is perhaps too small in this region. It should be noted, however, that a decided break in slope is evident in the σ_1^b obtained by Bos and Lynch at 1.9–2.0 eV and is also seen somewhat more weakly in the Benbow and Lynch results and in other data.[41] This corresponds almost precisely

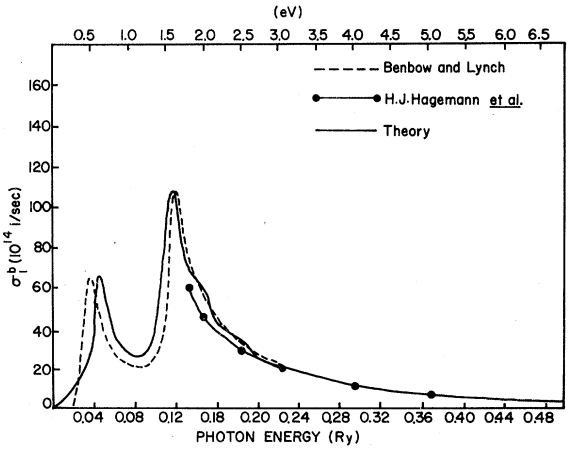

FIG. 7. Comparison between the theoretical broadened and experimentally obtained $\sigma_1^b(\omega)$ for Al.

to the broadened D structure.

The position of the calculated second peak is displaced from the empirical one by about 0.04 eV. The reason for this small discrepancy is that our parametrization was performed using the data of Bos and Lynch,[13] which place the peak at 1.60 eV. A larger discrepancy of 0.13 eV occurs in the location of the lower peak. It is not clear how significant this discrepancy is. In a region of such low ω it is very difficult to separate accurately the interband from the Drude contribution, which is quite large, and different separations lead to shifts in the peak position. To make such a separation it is, in effect, necessary to assume a form for $\sigma_1^b(\omega)$ in order to determine the parameters for the Drude contribution. For this purpose BL used the AS expression and this has a different form below the peak than we find. The AS spectrum falls rapidly to zero with nonvanishing values below the edge arising solely from the phenomenological broadening (finite τ). As we will show, the behavior of σ_1^b below the peak is dominated by real interband transitions which persist down to $\omega = 0$. An indication of the difficulties in the low ω region due to the above-mentioned problems is the fact that the empirically determined σ_1^b goes negative for ω below 0.25 eV.

Since the magnitude of the broadened curve between the peaks depends on the separation of as well as strengths of the peaks, the discrepancy in that region is attributable in good part to the uncertainties in peak positions. Considering the above-mentioned experimental uncertainties, the overall agreement is quite satisfactory.

B. Form of $\epsilon_2^b(\omega)$ for $\omega \to 0$

For ω well below the 0.5-eV peak there is a very weak contribution to ϵ_2^b from the broadening of the peak; there are, however, also contributions which come from an accidental degeneracy (crossing) of two bands on the ΓKWX plane around E_F. That transitions from these bands would occur down to $\omega = 0$ was first noted by Brust.[8] However, he did not specifically investigate the magnitude of these contributions to ϵ_2^b and his numerical calculations, which were on a relatively coarse grid, did not exhibit such contributions. Here we study them analytically. From Fig. 1 it can be seen that the degeneracies start at the Δ axis where Δ_5 and Δ_1 cross above E_F and continue across the plane to the Z axis where the Z_1 and Z_4 bands intersect near W and below E_F. Figure 6 shows the ΓKWX plane with its intersection of the second- and third-zone Fermi surfaces. The line of accidental degeneracies, which is dashed, runs through the point at which the two surfaces make contact.

To obtain the contributions to $\epsilon_2^b(\omega)$ from this region, we perform a $\vec{k}\cdot\vec{p}$ analysis. We let $\vec{q}$ be the wave vector measured from the degeneracy point at E_F, which is taken to be the zero of energy. The secular determinant associated with the 2×2 $\vec{k}\cdot\vec{p}$ Hamiltonian with matrix elements $H_{11(22)} = q^2 + 2\vec{q}\cdot\vec{P}_{11(22)}$ and $H_{12} = H_{21} = 2\vec{q}\cdot\vec{P}_{12}$ yields to lowest order in q the two energies

$$E_{\vec{k}+\vec{q}} = \vec{q}\cdot(\vec{P}_{11}+\vec{P}_{22}) \pm\{[\vec{q}\cdot(\vec{P}_{11}-\vec{P}_{22})]^2 + 4(\vec{q}\cdot\vec{P}_{12})^2\}^{1/2}, \tag{9}$$

where $\vec{P}_{ij}$ are the MEM's between the bands i and j. At the contact point, and all other points in the plane, the two bands are odd and even under reflection and, as a result, $\vec{P}_{11}$ and $\vec{P}_{22}$ lie in the plane while $\vec{P}_{12}$ is orthogonal to it. Making the (generally nonorthogonal) transformation $\vec{q}\cdot(\vec{P}_{11}+\vec{P}_{22}) = u$, $\vec{q}\cdot(\vec{P}_{11}-\vec{P}_{22}) = v$, and $\vec{q}\cdot\vec{P}_{12} = w/2$, we see that the interband energy is $2(v^2+w^2)^{1/2}$ and the JDOS is

$$\mathcal{J}(\omega) \propto \int dv \int dw \int_{-(v^2+w^2)^{1/2}}^{(v^2+w^2)^{1/2}} \delta(\omega - 2(v^2+w^2)^{1/2})\,du\,. \tag{10}$$

The limits on the integral over u result from the requirement that the upper level lie above E_F and the lower level below it. The integral is readily evaluated using cylindrical coordinates and one finds

$$\mathcal{J}(\omega) \propto \omega^2, \quad \epsilon_2^b(\omega) \propto \frac{\mathcal{J}(\omega)}{\omega^2} \propto \text{const.} \tag{11}$$

Thus we find the somewhat unexpected result that $\epsilon_2(\omega)$ is constant and $\sigma_1^b \propto \omega$ for small ω. This predicted behavior, which is not evident in the results of the previous calculations, is borne out in our numerical results for the unbroadened σ_1^b (see Fig. 4). It is seen that the constant $\epsilon_2^b(\omega)$ approaches is not small; it has a value of about 18.

When the spin-orbit interaction is turned on, the accidental degeneracy is split by an amount Δ and, as a result, $\epsilon_2^b(\omega)$ must vanish for $\omega < \Delta$. In Appendix C we study the threshold behavior of $\epsilon_2^b(\omega)$ with the spin-orbit interaction included, and we find that just above the threshold Δ, $\epsilon_2^b(\omega)$ is constant. Equation (11) should be viewed as the limit of this result for vanishingly small Δ. Vanishing of $\epsilon_2^b(\omega)$ at $\omega = 0$ is in accord with the requirement that $\epsilon_2^b(\omega)$ be an odd function of ω.[42] For Al $\Delta \sim 10^{-3}$ Ry, which for the optical experiments is essentially zero.

It should be noted that accidental degeneracies at E_F also occur in other polyvalent metals, e.g., in the hcp group-II metals. In those elements in which the magnitude of the spin-orbit interaction is small compared to the position of the lowest-

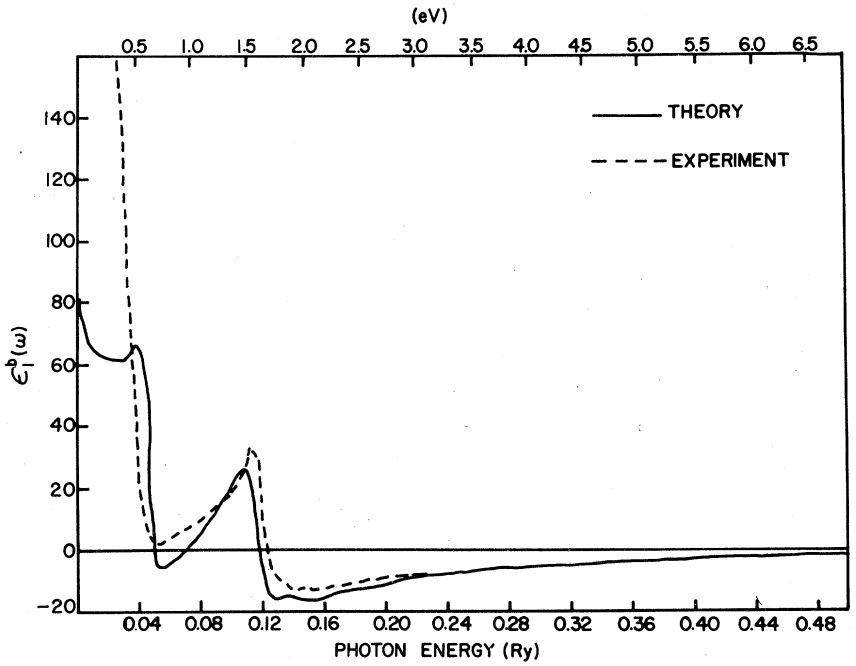

FIG. 8. Comparison between the $\epsilon_1^b(\omega)$ obtained in the present calculations and that obtained by fitting the Ashcroft-Sturm expression for $\epsilon_2^b(\omega)$ to the data.

energy peak in ϵ_2^b (e.g., in Be, Mg, and possibly Zn), contributions similar to those described above will occur.

The transitions discussed here will, of course, also contribute to $\epsilon_1^b(\omega)$. Figure 8 shows the ϵ_1^b curves obtained by the Kramers-Kronig relations using the ϵ_2^b obtained here and the one obtained by fitting the AS expressions to the data.[39] The large differences between the curves below approximately 0.04 Ry can readily be understood in terms of the differences in ϵ_2^b in the low-ω region. In this region, of course, $\epsilon_1^f(\omega)$ is very large so that the relative error in $\epsilon_1(\omega)$ due to neglect of the transitions considered here is not so dramatic. We estimate that at 0.3 eV the relative error is roughly 10% in Al. Larger errors would occur, and thus be appreciable, in materials in which the first peak falls at higher energies.[43]

V. CONCLUSIONS

The band structure of Al obtained in a first-principles APW calculation was empirically adjusted by the input of a few firmly established pieces of empirical data relating to the Fermi surface and band spacings. The approach used, which is a variant of the one used by Chen and Segall for the noble metals, involves the adjustment of the first-principles logarithmic derivatives. The fact that it was found to be accurate (yielding the correct Fermi surface and optical response) and to be fairly easily applied, suggests that it could be employed successfully for other nearly-free-electron metals as well as transition metals.

The interband contribution to the optical response function, $\sigma_1^b(\omega)$, was calculated with the inclusion of matrix elements. The origin of all structure has been elucidated. In particular, the region of the BZ contributing to the 0.5-eV peak, which involves general $\vec{k}$, was described more clearly than before.

A novel feature of the calculations is the study of the contributions of interband transitions between two bands which cross (in the absence of spin-orbit interaction) at the Fermi energy. An analytic $\vec{k}\cdot\vec{p}$ calculation shows that $\epsilon_2^b(\omega)$ is a non-vanishing constant as $\omega \to 0$, a result that is seen in our numerical results which level off below the 0.5-eV peak. This behavior is quite different than that given by the "parallel-band" model which has been used recently in analyzing measured spectra Similar behavior is expected to occur in other light polyvalent metals.

Our broadened calculated $\sigma_1^b(\omega)$ is in good agreement with the corresponding spectrum determined from measurements with respect to the location and magnitude of the structure and magnitude and shape of the featureless parts. It was suggested that the small discrepancies between the position of the low-energy peak may be due to difficulties associated with separating the interband contri-

TABLE II. Matrix elements of momentum (in $Ry^{1/2}$) for aluminum using the pseudo-wave-functions and APW wave functions.

$k\left(\frac{2\pi}{8a}\right)$	Transition	APW	Pseudopotential
044	2 → 3	0.7280	0.7778
055	2 → 3	0.7522	0.7775
066	1 → 2	0.1779	0.2127
	1 → 3	0.7422	0.7483
	2 → 3	0.2040	0.2014
018	1 → 2	0.7749	0.7776
	3 → 4	0.6559	0.7776
028	1 → 2	0.7703	0.7768
	3 → 4	0.7115	0.7768
038	1 → 2	0.7595	0.7729
	3 → 4	0.7338	0.7729
048	1 → 3	0.5298	0.5502
	1 → 4	0.5352	0.5502
	2 → 3	0.5298	0.5502
	2 → 4	0.5352	0.5502
	3 → 4	0.3792	0.3891
007	1 → 2	0.1716	0.1809
118	1 → 2	0.7739	0.7772
008	1 → 2	0.7762	0.7778
444	1 → 2	0.3814	0.3884

butions from the very large Drude component in that region. We also note that the use of the parallel-band result (in the process of determining the Drude parameters), which does not have the correct behavior at low ω, could also lead to errors in this region.

An extensive comparison of pseudopotential momentum matrix elements with accurate APW values show differences for the larger matrix elements which are generally about 5% with maximum errors reaching about 20%. Part of the errors can be attributed to the limited four-plane-wave set.

ACKNOWLEDGMENTS

We thank Professor William L. Gordon for discussions about experimental aspects related to this work and to Dr. D. W. Lynch for kindly providing us with his numerical optical data. One of us (B.S.) thanks the Max Planck Institut für Festkörperforschung for its hospitality during the period that this paper was written. This work was supported in part by the National Science Foundation under Grant No. DMR76-21550 A01.

APPENDIX A: COMPARISON OF PSEUDOPOTENTIAL AND APW MATRIX ELEMENTS OF MOMENTUM

Our calculations for this study used Snow's potential[5] and obtained for the pseudopotential fit of the l nds the parameters $\alpha = 0.9478$ (inverse mass), $V(1,1,1) = 0.00943$ Ry, and $V(2,0,0) = 0.03849$ Ry (lattice constant $a = 7.6529$ a.u.). The pseudo-wave-function for band n at $\vec{k}$ is given by

$$\gamma_n(\vec{k}) = \sum_i v_{n\vec{k}}(\vec{K}_i) \exp[i(\vec{k}+\vec{K}_i)\cdot\vec{r}] , \tag{A1}$$

where $(a/2\pi)\vec{K}_i = (0,0,0)$, $(0,0,\bar{2})$, $(\bar{1},\bar{1},\bar{1})$, and $(1,\bar{1},\bar{1})$. The above set of plane waves yields properly symmetrized pseudo-wave-functions only at the point W.

It can be shown using Ehrenfest's theorem with plane-wave expansions [as in (A1)] that the MEM's are given by

$$2\vec{P}_{mn}(\vec{k}) = \sum_{i,j} v_{m\vec{k}}(\vec{K}_i) \frac{\partial H(\vec{k})_{ij}}{\partial \vec{k}} v_{n\vec{k}}(\vec{K}_j) , \tag{A2}$$

where $H(\vec{k})_{ij}$ is the matrix element of the Hamiltonian between the plane waves with reciprocal-lattice vectors $\vec{K}_i$ and $\vec{K}_j$. In the local pseudopotential approach

$$H(\vec{k})_{ij} = \alpha(\vec{k}+\vec{K}_i)^2\delta_{ij} + V(\vec{K}_j - \vec{K}_i) \tag{A3}$$

in a restricted basis set of the type employed here. It is apparent that in this approach the momentum operator assumes the form $-i\alpha\vec{\nabla}$ in place of $-i\vec{\nabla}$ reflecting the fact that the overall band curvature is given by α and not 1.

We have calculated the MEM's given by Eqs. (A2) and (A3) at a number of $\vec{k}$'s. The comparison of the "larger" of these (i.e., greater than 0.1) and the corresponding APW MEM's is given in Table II.

APPENDIX B: FERMI-SURFACE PARAMETRIZATION

Anderson and Lane made a least-squares fit to the measured cross-sectional areas of the Fermi

TABLE III. Second- and third-zone "calipers" in units of $(2\pi/8a)(x,y,z)$.

Level	2nd-zone calipers	Level	3rd-zone calipers
Δ_1	0.0, 0.0, 7.0488	Σ_1	0.0, 5.6540, 5.6540
Σ_3	0.0, 4.6202, 4.6202	Z_4	0.0, 3.2202, 8.0
Λ_1	2.7908, 2.7908, 2.7908	Z_1	0.0, 3.5453, 8.0
$\Gamma KWX-$	0.0, 4.0, 5.3834	S_1	1.6383, 1.6383, 8.0
$\Gamma LUX+$	2.1659, 2.1659, 4.3317	(1,1,1) face	0.2958, 5.7042, 6.0

surface using a 4-OPW model.[7] Their best fit was obtained with $V(1,1,1)=0.018$ Ry, $V(2,0,0)=0.062$ Ry, and an effective mass of 1.0. We have used their model to compute the calipers shown in Table III. The states Σ_3, Z_4, and ΓKWX – have no $l=0$ component. With the $\vec{k}$ set to the values of the calipers for each of the states, we varied v_1 with v_2 fixed until the APW secular determinant vanished at E_F. This was done for a range of v_2 giving curves of v_2 vs v_1 for each state. It turned out that these curves were essentially identical and thus gave a functional relation between v_2 and v_1. A similar procedure was followed with the Δ_1, Σ_1, and (1,1,1) face calipers except that v_0 was varied with fixed v_1. The resulting plots of v_1 vs v_0 were found to intersect in a very small region. The uncertainty in determining the intersection point and hence the v_l's is approximately 1 mRy.

APPENDIX C: THRESHOLD BEHAVIOR OF $\epsilon_2^b(\omega)$ IN THE PRESENCE OF SPIN-ORBIT INTERACTION

Here the $\vec{k}\cdot\vec{p}$ Hamiltonian is augmented by the spin-orbit interaction $(2mc)^{-2}\hbar\vec{\sigma}\cdot(\nabla V\times\vec{p})$. As the four eigenfunctions of the unperturbed problem we take $\psi_{1(2)}=\phi_+\alpha(\beta)$ and $\psi_{3(4)}=\phi_-\alpha(\beta)$, where $\phi_{+(-)}$ is even (odd) under reflection and α (β) is the spin-up (-down) function. Using the same notation as in Sec. IV and taking the x axis to be normal to the plane, we find using reflection symmetry that the Hamiltonian matrix is given by

$$H_{11}=H_{22}=2\vec{q}\cdot\vec{P}_{11},$$
$$H_{33}=H_{44}=2\vec{q}\cdot\vec{P}_{22},$$
$$H_{12}=H_{34}=0,\quad H_{13}=H_{24}=2\vec{q}\cdot\vec{P}_{12},$$

and

$$-H_{23}^*=H_{14}=G_{+-}^z-iG_{+-}^y=2F,$$

where $4|F|=\Delta$, with

$$(2mc)^{-2}\hbar\langle\phi_+|(\vec{\nabla}V\times\vec{P})_s|\phi_-\rangle=G_{+-}^s\ (s=y,z).$$

The secular equation has two doubly degenerate roots which to lowest order in $\vec{q}$ are

$$E(\vec{k}+\vec{q})_{+-}=\vec{q}\cdot(\vec{P}_{11}+\vec{P}_{22})\pm\{\vec{q}\cdot(\vec{P}_{11}-\vec{P}_{22})+4[(\vec{q}\cdot\vec{P}_{12})^2+|F|^2]\}^{1/2}. \tag{C1}$$

In terms of the u, v, and w of Sec. IV, we find that the interband energy is

$$\omega(u,v,w)=2(v^2+w^2+4|F|^2)^{1/2} \tag{C2}$$

and the Fermi cutoff conditions are $u\geq-\omega/2$ and $u\leq\omega/2$. Aside from the presence of the spin-orbit splitting term $4|F|^2$, Eqs. (C1) and (C2) are the same as the previous ones. By converting to cylindrical coordinates with the axis along u the JDOS integral

$$g(\omega)=\int du\int dv\int dw\,\delta(\omega-\omega(u,v,w)) \tag{C3}$$

is easily shown to be proportional to ω^2 for $\omega\geq 4|F|$ and to vanish for lower ω. Thus, immediately above threshold we again find that ϵ_2^b is constant.

---

*Present address: University of Dayton Research Institute, Dayton, Ohio 45469.

†On leave at the Max Planck Institut für Festkörperforschung, 7000 Stuttgart 80, Federal Republic of Germany.

[1]A.-B. Chen and B. Segall, Phys. Rev. B 12, 600 (1975).

[2]V. Heine, Proc. R. Soc. London, Ser. A 240, 361 (1957).

[3]W. A. Harrison, Phys. Rev. 118, 1182 (1960).

[4]B. Segall, Phys. Rev. 124, 1797 (1961).

[5]E. C. Snow, Phys. Rev. 158, 683 (1967).

[6](a) N. W. Ashcroft, Philos. Mag. 8, 2055 (1963); (b) S. P. Singhal and J. Callaway, Phys. Rev. B 16, 1744 (1977).

[7]J. R. Anderson and S. S. Lane, Phys. Rev. B 2, 298 (1970).

[8]D. Brust, Phys. Rev. B 2, 818 (1970).

[9]H. Ehrenreich, H. R. Phillipp, and B. Segall, Phys. Rev. 132, 1918 (1963).

[10]The magnitude of ϵ_2 was underestimated by a factor of 3.

[11]G. Dresselhaus, M. S. Dresselhaus, and D. Beaglehole, *Electronic Density of States*, edited by L. H. Bennett, (Natl. Bur. Stand. Spec. Publ. #323, Gaithersburg, MD, 1971), p. 33.

[12]N. W. Ashcroft and K. Sturm, Phys. Rev. B 3, 1898 (1971).

[13]L. W. Bos and D. W. Lynch, Phys. Rev. Lett. 25, 156 (1970).

[14]R. L. Benbow and D. W. Lynch, Phys. Rev. B 12, 5615 (1975).

[15]A. G. Mathewson and H. P. Myers, Phys. Scr. 4, 291 (1971).

[16]J. C. Slater, Phys. Rev. 51, 846 (1937).

[17]L. F. Mattheiss, Phys. Rev. 133, A1399 (1964).

[18]P. O. Löwdin, Adv. Phys. 5, 1 (1956).

[19]A. C. Switendick (unpublished).

[20]B. Segall, Phys. Rev. 125, 109 (1962).

[21]G. A. Burdick, Phys. Rev. 129, 168 (1963).

[22]J. F. Janak, A. R. Williams, and V. L. Moruzzi, Phys. Rev. B 4, 1522 (1975).

[23]A.-B. Chen, Phys. Rev. B 14, 2384 (1976).

[24]W. Beeferman and H. Ehrenreich, Phys. Rev. B 2, 364 (1970).
[25]J. Appelbaum, Phys. Rev. 144, 435 (1966).
[26]A. O. E. Animalu, Phys. Rev. 163, 557 (1967); 163, 562 (1967).
[27]G. Martinez, M. Schlüter, and M. L. Cohen, Phys. Rev. B 11, 660 (1975).
[28]G. Gilat and L. J. Raubenheimer, Phys. Rev. 144, 390 (1966).
[29]R. J. Jelitto, J. Phys. Chem. Solids 30, 609 (1969).
[30]A.-B. Chen and B. Segall, Solid State Commun. 17, 1557 (1975); 18, 149 (1976).
[31](a) U. von Barth and L. Hedin, J. Phys. C 5, 1629 (1972); (b) we note that the self-consistent calculation of Singhal and Callaway, Ref. 6(b), yields a value of 1.4 eV for the energy of the measured 1.6-eV absorption peak in aluminum. This calculation which used the LDF formalism, however, did not include a correlation contribution to the potential; (c) D. R. Hamann, Phys. Rev. Lett. 42, 662 (1979); A. Zunger and M. L. Cohen, Phys. Rev. B 20, 4082 (1979); A. Zunger and A. J. Freeman, *ibid.* 15, 5049 (1976); D. Glötzel, B. Segall, and O. K. Anderson, Solid State Commun. 36, 403 (1980).
[32]Because of the E dependence of the potential the wave functions of the same l are not strictly orthogonal. This could complicate, e.g., the calculation of the MEM's. However, as noted the E dependence is quite weak and, as a result, we expect that corrections associated with these efforts are unimportant.
[33]C. O. Larson and W. L. Gordon, Phys. Rev. 156, 703 (1967).
[34]H. Neddermeyer and G. Wiech, Phys. Lett. 31A, 17 (1970).
[35]N. E. Phillips, Phys. Rev. 114, 676 (1959).
[36]See P. B. Allen and M. L. Cohen, Phys. Rev. 187, 525 (1969), and references cited therein.
[37]H. Ehrenreich and H. R. Philipp, Phys. Rev. 128, 1622 (1962).
[38]W. A. Harrison, Phys. Rev. 147, 467 (1966).
[39]These data, which did not appear in Ref. 14, were kindly supplied to us by Dr. Lynch.
[40]H. J. Hagemann, W. Gudat, and C. Kunz, Report No. DESY SR-74/7 (1974).
[41]H. E. Bennett, M. Silver, and E. J. Ashley, J. Opt. Soc. Am. 53, 1089 (1963).
[42]J. Tauc, in *The Optical Properties of Solids, Proceedings of the International School of Physics, "Enrico Fermi", Course* 34, edited by J. Tauc (Academic, New York, 1966), p. 66.
[43]The errors would mainfest themselves in the Drude parameters.